

Optimal optomechanical cavity setups with highly reflecting membranes

Georg Enzian,¹ Eugene S. Polzik,¹ and Alexander K. Tagantsev^{2,*}

¹*Niels Bohr Institute, Quantum Optics Laboratory - QUANTOP,
Blegdamsvej 17, DK-2100 Copenhagen, Denmark*

²*Swiss Federal Institute of Technology (EPFL), School of Engineering,
Institute of Materials Science, CH-1015 Lausanne, Switzerland*

(Dated: November 23, 2023)

Abstract

Highly reflecting mechanically compliant membranes based on photonic-crystal patterns have recently gained increasing attention within cavity optomechanics due to their prospects of reaching high coupling rates in membrane-in-the-middle experiments. Here we present an analysis and comparison of four different setups in which highly reflecting membranes can be employed for cavity optomechanics, and discuss optimal choices w.r.t. the figures of merit cooperativity and efficiency-weighted cooperativity. The analysis encompasses three different types of membrane-in-the-middle setups (membrane-at-the-edge, membrane-in-the-actual-middle, and membrane-at-the-back), as well as the simple Fabry-Perot cavity. Interestingly, we identify and propose the membrane-at-the-back setup as an optimal choice in the limit of negligible membrane parasitic loss, which can reach enormous enhancements of optomechanical cooperativity, and if implemented with a low-loss membrane would pave the way to nonlinear optomechanics in the quantum regime.

* alexander.tagantsev@epfl.ch

I. INTRODUCTION

An optical cavity with a mechanically compliant membrane placed inside it is a widely used optomechanical setup. Its typical realization is the so-called "membrane-in-the-middle" cavity (MIM), which consists of a Fabry-Perot optical cavity where the membrane is placed close to its middle [1–9]. In terms of Fig. 1, for such a configuration, the distance x is set close to $l/2$. Recently, it was identified [10] that, if the membrane is highly reflecting and properly positioned close to the input mirror, the optomechanical coupling constants of the system can be appreciably increased compared to the membrane-in-the-middle configuration. Such a configuration was called "membrane-at-the-edge" (MATE).

In this paper, we theoretically address the configuration where a highly reflecting membrane is positioned close to the backstop mirror, which we call "membrane-at-the-back" (MAK). We will compare the optimized optomechanical performance of the three afore-

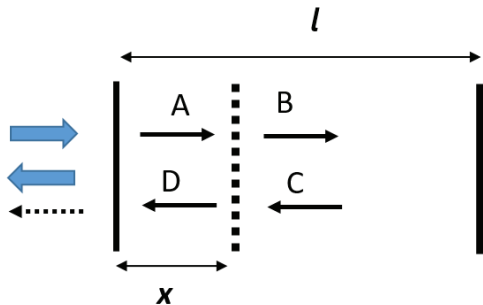


FIG. 1. A one-sided cavity with a mechanical semitransparent membrane set inside it. The dashed line represents the membrane, the thin solid line represents the semitransparent input mirror, the thick solid line represents the perfectly reflecting back-stop mirror, the thick arrows represent the pump light, and the dashed arrow represents the detected light. The waves inside the cavity are shown with arrows which are marked with their complex amplitudes.

mentioned configurations using the optomechanical cooperativity, as well as the efficiency-weighted cooperativity as figures of merit. Only the dispersive optomechanical coupling, as typically dominating the systems, is taken into account.

In contrast to the previous theoretical considerations of an optical cavity with a membrane inside [1, 2, 10], we have incorporated the parasitic scattering from the membrane in our consideration while neglecting the parasitic scattering from the coupling mirror, which we

assume to be much weaker than that from the membrane. We have demonstrated that, in the case of a highly reflecting membrane, even a small amount of parasitic scattering from the membrane may have an essential impact on the cooperativity of the system.

In the case of a highly reflecting membrane, the spectrum of the cavity is close to the superposition of those of the two subcavities, being strongly affected near the crossing points of these spectra by the effect of avoided crossing. At the avoided-crossing points, the dispersive optomechanical coupling vanishes. Evidently, halfway between these points, the suppressing effect of the avoided crossing on the dispersive coupling is minimal. Being interested in the best performance of the system, the consideration in the paper will be focused on these "halfway" points.

We will show that, for highly reflecting membranes, in terms of the cooperativity, MAK is always appreciably advantageous compared to MIM while, depending on the parameters of the system, MAK is either appreciably advantageous compared to MATE or yields a performance which is very close to that of MAK.

We will also compare the MAK scheme against the simple Fabry-Perot cavity (FP), with the highly reflecting membrane in the role of the coupling mirror. We will show that, depending on the parameters of the systems, MAK can be more or less advantageous than the aforementioned FP of the length equal to the above separation.

II. SYSTEM MODEL

To be specific, we set the following scattering matrices:

$$\begin{pmatrix} it & -r \\ -r & it \end{pmatrix} \quad (1)$$

for the input mirror

$$\begin{pmatrix} 0 & -1 \\ -1 & 0 \end{pmatrix} \quad (2)$$

for the backstop mirror, and

$$\begin{pmatrix} t_m e^{i\varphi_t} & r_m e^{i\varphi_r} \\ r_m e^{i\varphi_r} & t_m e^{i\varphi_t} \end{pmatrix} \quad (3)$$

for the membrane, where the amplitude transmission coefficients are on the diagonals. Here all parameters are set as real and positive while

$$t^2 + r^2 = 1 \quad \text{and} \quad e^{2i(\varphi_r - \varphi_t)} = -1 \quad (4)$$

The finesse of the cavity is assumed to be high:

$$t \ll 1 \quad (5)$$

Though the treatment of cavities with a membrane inside is typically done neglecting parasitic scattering against the membrane, i.e. assuming $t_m^2 + r_m^2 = 1$, we will incorporate it into the consideration since as will be seen below such a scattering may strongly affect behaviors of the system addressed. Specifically we set

$$t_m^2 + r_m^2 = 1 - t_s^2 \quad (6)$$

where t_s^2 is the power scattering coefficient associated with the aforementioned scattering.

Throughout the paper we will restrict ourselves to the case of high reflecting membrane, i.e.

$$t_m^2 \ll 1. \quad (7)$$

As it is seen from Eqs.(2) and (4) we neglect the parasitic scattering against the coupling mirror and a finite transmission of the backstop mirror. This is justified under reasonable assumptions that the above scattering is much weaker than the coupling mirror transmission while the power transmission of the backstop is much smaller than t_s^2 .

III. BASIC FEATURES OF AN OPTICAL CAVITY WITH A HIGHLY REFLECTING MEMBRANE INSIDE

Let us address basic features of an optical cavity with a highly reflecting membrane inside. Let us start from the case of a perfectly reflecting membrane ($t_m = 0$). In this case, the resonance spectrum of the system for any position of the membrane is just the sum of spectra of its right and left sub-cavities as shown in figure 2. The resonance frequencies of modes of the left part ω_L decrease with increasing x while those of modes of the right part ω_R increase. Hereafter we will term such modes ω_L modes and ω_R modes, respectively. For small but finite t_m , the spectrum shown in Fig. 2 provides a good approximation for

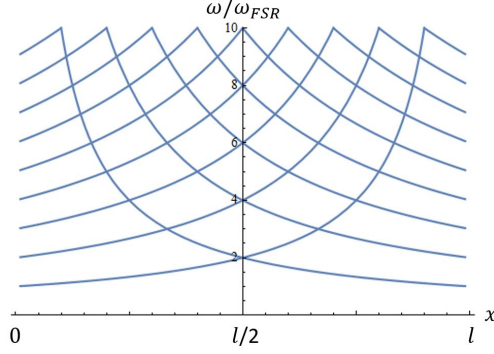


FIG. 2. The spectrum of an optical cavity with a perfectly reflecting membrane inside ($r_m = 1$) as a function of the membrane position. The phase shift at reflection from the membrane is set as $\varphi_r = \pi$. $\omega_{\text{FSR}} = \pi c/l$ is the free spectral range of the empty cavity.

the spectrum except the vicinity of the crossing points where an avoided crossing takes place, resulting in the formation of a small gap. Away from avoided crossing points, we can still keep unambiguous nomenclature, ω_L mode and ω_R mode, to classify the modes. The modification of the spectrum caused by a variation of t_m is illustrated in Fig. 3. Here the

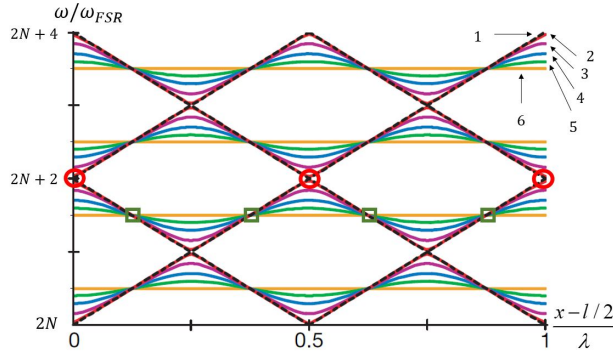


FIG. 3. A part of the spectrum of an optical cavity with a semitransparent membrane inside for high order cavity resonances ($N \gg 1$ is integer) plotted for different values of its amplitude transmission coefficients t_m : 1 (1), 0.95 (2), 0.8 (3), 0.48 (4), 0.1 (5), and 0 (6). ω_{FSR} is the free spectral range of the empty cavity. The phase shift at reflection from the membrane is set as $\varphi_r = \pi$. Three crossing points are marked with circles. Four "r" points are marked with squares. Figure is based on the results from Ref. [4].

effect of avoided crossings at the crossing points is seen. Three crossing points are marked with circles.

An important feature of the avoided crossing is that this effect is the stronger, the stronger the displacement of the membrane from the middle of the cavity. This can be readily demonstrated starting from the following well-known equation

$$\cos(kl + \varphi_r) = -r_m \cos(2kx - kl), \quad (8)$$

for the resonant wave vector k of an optical cavity with a semitransparent mirror inside (see e.g. [10]), which is written neglecting the energy decay in the cavity. To evaluate the strength of the avoided crossing, we evaluate the gap induced by a small t_m at the crossing point of the decoupled ω_L and ω_R modes. A form of equation (8) that is proper for further analysis reads

$$\cos[k(l - x) + \varphi_r/2] \cos(kx + \varphi_r/2) = \frac{t_m^2}{4} \cos(2kx - kl) \quad (9)$$

such that the membrane position x_0 and the resonance wave vector k_0 , corresponding to a crossing point. At these points, both subcavities taken decoupled are on resonance such the both cosines form (9) should be equal to zero:

$$\cos[k_0(l - x_0) + \varphi_r/2] = 0 \quad \text{and} \quad \cos(k_0x_0 + \varphi_r/2) = 0. \quad (10)$$

Next, looking for the solution to equation (9) in the form $x = x_0$ and $k = k_0 + \delta k$, we find, in the limit of small t_m , that

$$\delta k^2 \propto \frac{t_m^2}{x_0(l - x_0)}, \quad (11)$$

implying that the effect of the avoided crossing increases once the membrane approaches one of the cavity mirrors.

Solution to equations (10) also yields

$$\omega_0 = \omega_{\text{FSR}} \left(N - \frac{\varphi_r}{\pi} \right) \quad (12)$$

for the frequency of the crossing points $\omega_0 = ck_0$, where $\omega_{\text{FSR}} = \pi c/l$ is the free spectral range of the empty cavity, c is the speed of light, and N is integer.

Another remarkable feature of the system, which is seen from Fig. 3, is that the positions of the points where the dispersion curves of the decoupled modes (the straight lines in the figure) cross the dispersion curves of the system (at finite membrane transmission t_m) are not sensitive to the value of t_m . In Fig. 3, four of such points are marked with squares. With a variation of t_m , the $\omega(x)$ curves “locally rotate” about such points. We term these

points r-points. One can readily show that the positions of such points are independent of the transmission of the membrane.

To be specific let us consider the r-points formed by the intersection of the $\omega(x)$ curves for the ω_L mode calculated at $t_m = 0$ and $t_m \neq 0$. Since we are on the resonance curve for the x -long part of the cavity taken decoupled from the other part, the phase shift on reflection from the membrane equals φ_r . Thus, taking into account that the round-trip phase variation along any loop should be equal to 2π times an integer, we can write

$$e^{2ikx+\pi+\varphi_r} = 1. \quad (13)$$

For the $l - x$ -long part, we can also write the following round-trip phase condition

$$e^{2ik(l-x)+\pi+\mu} = 1, \quad (14)$$

where μ is the phase shift at the reflection from the x -long part. Since the $l - x$ -long part taken decoupled is not on resonance $\mu \neq \varphi_r$. These two equations specify the positions of the corresponding r-points. On the other hand, one readily checks that the phase shift on reflection from a one-sided cavity on resonance is independent of transmission of the input mirror (see Appendix A). For our setting

$$\mu = \varphi_r - \pi. \quad (15)$$

Thus, μ is independent of the membrane transmission, implying the independence of positions of the r-points.

Solving equations (13), (14), and (15) also yields

$$\omega_r = \omega_{\text{FSR}} \left(\frac{1}{2} + N - \frac{\varphi_r}{\pi} \right) \quad (16)$$

for the frequency of r-points.

Figure 4 illustrates the relative position of the points of avoided crossing and r-points on an ω_L branch of the spectrum. It is seen that, in frequency, these are separated by $\omega_{\text{FSR}}/2$ as it follows from equations (12) and (16). In other words, each r-point lies in the middle between two neighboring points of avoided crossing. The avoided crossing obviously results in a reduction of the slopes of the $\omega(x)$ curves and, as a result, in a reduction of the optomechanical coupling. It is clear that the middle position of the r-points between

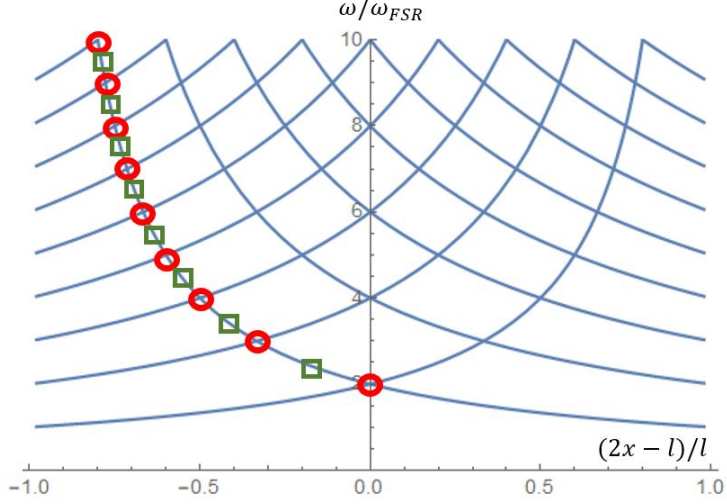


FIG. 4. Schematic of the spectrum of an optical cavity as a function of the membrane position. The impact of avoiding crossings is not explicitly shown. For one ω_L mode, the places where the avoided crossing occurs are marked with the circles while the r-points are marked with the squares. ω_{FSR} is the free spectral range of the empty cavity. The phase shift at reflection from the membrane is set as $\varphi_r = \pi$.

the neighboring points of avoided crossing makes the r-points favorable in terms of such a coupling. For this reason, in the further discussion, we will focus on these points.

Here it is also instructive to note that at the r-points one of the sub-cavities is on resonance while the other is on antiresonance. For ω_L modes, it is clear from rewriting Eqs.(13), (14), and (15) as follows

$$e^{-2ik_0(l-x)-i\varphi_r} = 1, \quad e^{-2ik_0x-i\varphi_r} = -1. \quad (17)$$

Similar expressions can be readily shown for ω_R modes:

$$e^{-2ik_0(l-x)-i\varphi_r} = -1, \quad e^{-2ik_0x-i\varphi_r} = 1 \quad (18)$$

implying the same for this mode either.

Next, for the r-points, we evaluate the ratio of the field intensity in one part of the cavity to that in the other part. We will first consider this for an ω_L mode. Based on equation (3), we consider the following complex amplitude balance equation at the membrane (compare Fig. 1)

$$B = t_m e^{i\varphi_s} A + r_m e^{i\varphi_r} C. \quad (19)$$

Since, at the r-points considered, the x-long part taken decoupled is on resonance, using (15), we can write

$$B = e^{i(\varphi_r - \pi)} C. \quad (20)$$

Combining equations (19) and (20), in the limit $t_m \ll 1$, we find

$$\frac{|B|^2}{|A|^2} = \frac{T_m}{4}, \quad (21)$$

where $T_m = t_m^2$ is the power (intensity) transmission while $|A|^2$ and $|B|^2$ are the intensities in the x-long and l-x-long parts of the cavity, respectively.

For the r-points of the ω_R mode, similar calculations yield

$$\frac{|B|^2}{|A|^2} = \frac{4}{T_m}. \quad (22)$$

As seen from Fig. 3, once the membrane is close to the middle of the cavity, for small t_m , the slope of the $\omega(x)$ curves at the r-points is hardly affected by the avoided crossing. However, as was shown above, the effect of the avoided crossing increases when the membrane approaches one of the cavity mirrors. Thus, for small distances between the membrane and the mirror, the impact of the avoided crossing on the aforementioned slope may become appreciable. Let us introduce the critical membrane-mirror separation, we term it x_{int} , at which this happens. ("Int" means interaction of the small cavity the large one.) We mean that, at $x_{\text{int}} \ll x \ll l$ (we discuss the ω_L mode), such impact is negligible while, at $x \ll x_{\text{int}} \ll l$, it is strong. One may say that an appreciable impact of the avoided crossing, i. e. an appreciable deviation of the dispersion curve from that of the decoupled subcavity, occurs when the mode "feels" the difference between a perfectly reflecting membrane and our membrane with a finite transmission t_m . In other words, this occurs when an appreciable fraction of the mode energy is not confined between the membrane and the nearest mirror. On the lines of the said above we determine x_{int} from the condition that, at $x = x_{\text{int}}$, the mode energies stored in the two parts of the cavity are equal.

Such a condition evidently reads

$$x|A|^2 = (l - x)|B|^2 \quad (23)$$

yielding, in view of $x \ll l$ and equation (21),

$$x_{\text{int}} = l \frac{T_m}{4}. \quad (24)$$

Using equation (22), one finds that equation (24) also applies to the ω_R mode, x_{int} being the critical separation from the backstop mirror.

IV. DISPERSIVE COUPLING FOR AN OPTICAL CAVITY WITH A HIGHLY REFLECTING MEMBRANE INSIDE

In this section we consider the dispersive optomechanical coupling at the r-points. We define the dispersive coupling constant of the system as follows

$$g_0 = -\frac{d\omega_c}{dx}x_{\text{zpf}} \quad (25)$$

where ω_c is the resonance frequency of the system and x_{zpf} is the amplitude of zero-point fluctuations. Let us first address g_0 of the ω_L mode. According to section III, at $l - x_{\text{int}} \gg x \gg x_{\text{int}}$, the dispersive coupling for the decoupled ω_L mode, i.e. at $t_m = 0$, provides a good approximation for that at finite t_m , implying

$$g_0 = \frac{\omega_c}{x}x_{\text{zpf}}. \quad (26)$$

Here, the $1/x$ increase of g_0 at $x \rightarrow 0$ results from the confinement of the mode energy in a decreasing volume. At x approaching x_{int} , this trend saturates such that one can reasonably suppose that at $x \ll x_{\text{int}}$

$$g_0 = \frac{\omega_c}{x_{\text{int}}}x_{\text{zpf}}, \quad x_{\text{int}} = l\frac{T_m}{4}. \quad (27)$$

The result given by (27) is consistent with the enchanted value of g_0 , which was identified for the system in reference [10].

Such a heuristic result is readily supported by direct calculations. We rewrite the resonance equation (8) in the following equivalent form (see Appendix B)

$$(r_m + e^{-2ik(l-x)-i\varphi_r})(r_m + e^{-2ikx-i\varphi_r}) + 1 - r_m^2 = 0 \quad (28)$$

and calculate $\frac{dk}{dx}$ at k satisfying Eq.(17) Next using (25) and taking into account that $T_m \ll 1$ we find (see Appendix B)

$$g_0 = \frac{\omega_c}{x + x_{\text{int}}}x_{\text{zpf}}, \quad (29)$$

justifying (27).

The above heuristic argument holds for the ω_R mode while, the direct calculation involving (28) and (18) yields (see Appendix B)

$$g_0 = -\frac{\omega_c}{l - x + x_{\text{int}}}x_{\text{zpf}}. \quad (30)$$

Next, basing on equations (29) and (30), in Table I, we summarize the values of g_0 for three regimes, namely, where $x \ll x_{\text{int}}$, $|x - l/2| \ll l$, and $l - x \ll x_{\text{int}}$, which we label MATE, MIM, and MAK for the membrane-at-the-edge, membrane-in-the-middle, and membrane-at-the back systems, respectively. Note that the values for MATE and MAK given in this table to within a factor of 1/2 holds for results for the membrane/mirror separation equal to x_{int} .

	MATE	MIM	MAK
ω_L	$2/T_m$	1	1/2
ω_R	1/2	1	$2/T_m$

TABLE I. The absolute values of the dispersive optomechanical coupling constants normalized to the MIM coupling constant $g_0/[\omega_c/(l/2) \cdot x_{\text{zpf}}]$ for the ω_L and ω_R modes at r-points for three configurations: $x \ll x_{\text{int}}$, $|x - l/2| \ll l$, and $l - x \ll x_{\text{int}}$, which are labeled as MATE, MIM, and MAK, respectively. T_m is the power transmission coefficient of the membrane. The values for MATE and MAK to within a factor of 1/2 holds for results for the membrane/mirror separation equal to x_{int} . The results are valid for the r-points of the spectrum.

As the dispersive coupling constants are only determined by the dependence of the cavity eigenfrequencies on membrane position and not by the dissipation, the symmetry between MATE and MAK is apparent in Table I, i.e. w.r.t. coupling, there is no difference between MATE and MAK.

V. CAVITY LINEWIDTH AND COOPERATIVITY FOR AN OPTICAL CAVITY WITH A HIGHLY REFLECTING MEMBRANE INSIDE

The dispersive coupling constant g_0 evaluated above does not represent, in general, a reliable optomechanical figure of merit. An appropriate figure of merit for mechanical sensing [11] and optomechanical squeezing [12] is the so-called single-photon cooperativity, which reads

$$C = \frac{4g_0^2}{\kappa\gamma_m}, \quad (31)$$

where κ is the optical decay rate and γ_m is the mechanical decay rate. C is a fully appropriate parameter in the case where the linewidth of the system is controlled only by the energy

leakage though the coupling mirror. However once the parasitic scattering against the membrane is involved, after stating that the linewidth can be decomposed into a contribution from external coupling and parasitic loss

$$\kappa = \kappa_{\text{ext}} + \kappa_s , \quad (32)$$

we can define the efficiency-weighted cooperativity

$$C_\eta = \eta C = \frac{4g_0^2 \kappa_{\text{ext}}}{(\kappa_{\text{ext}} + \kappa_s)^2 \gamma_m} \quad (33)$$

where we introduced the coupling efficiency η as

$$\eta = \frac{\kappa_{\text{ext}}}{\kappa}. \quad (34)$$

A. Simple estimates and qualitative arguments

We will start a more detailed analysis from a comparison and the cooperativity performance MATE, MIM, and MAK in the standard framework [1] [10] with the parasitic scattering against the membrane neglected, i.e. we set $t_s = 0$, c.f. Eq.(6), and for the regime where the membrane separation from the adjacent mirror is much smaller than $x_{\text{int}} = l \frac{T_m}{4}$. We will address the ω_R for MAK and ω_L for MATE since, as seen from Table I, these are the situations of interest.

The optical decay rate of MATE, MIM, and MAK can be readily found from the field distributions in these systems shown in Fig.5 and the standard definition (see e.g. [10]) of the decay rate:

$$\kappa = \frac{\text{dissipated power}}{\text{stored energy}} = \frac{ct^2 W(0)}{2l \bar{W}}, \quad (35)$$

where $W(0)$ and \bar{W} are the optical field intensity at the input mirror and the optical field intensity averaged over the cavity. Figure 5 illustrates the relations between the field intensities given by Eqs. (21) and (22). For MIM obviously:

$$\begin{aligned} W(0) &\approx 2\bar{W} & \text{for } \omega_L, \\ W(0) &\approx \frac{T_m}{2}\bar{W} & \text{for } \omega_R. \end{aligned} \quad (36)$$

As for MATE and MAK, taking into account that, in the addressed regime where the membrane separation from the adjacent mirror is much smaller than x_{int} , the energy of the

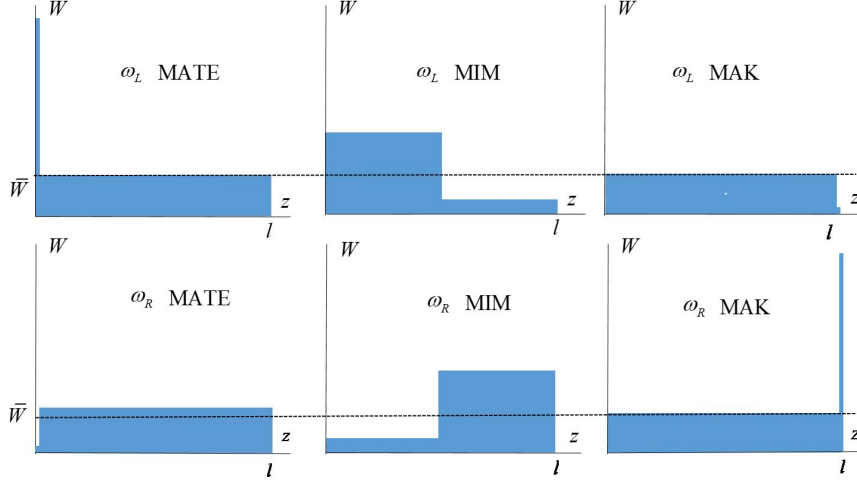


FIG. 5. The distribution of the field intensity in the MATE, MIM, and MAK configurations at r-points for the ω_L and ω_R modes. \bar{W} denotes the field intensity averaged over the cavity. For MATE and MAK, the regime where the membrane separation from the adjacent mirror is much smaller than $x_{\text{int}} = l\frac{T_m}{4}$ is considered. Figure is not to scale.

mode is mainly stored in the larger subcavities, one finds that for MATE

$$\begin{aligned} W(0) &\approx \frac{4}{T_m}\bar{W} & \text{for } \omega_L, \\ W(0) &\approx \frac{T_m}{4}\bar{W} & \text{for } \omega_R. \end{aligned} \quad (37)$$

while in MAK for both modes

$$W(0) \approx \bar{W}. \quad (38)$$

Next using the above results, those from Table I, and Eqs. (35) and (31) we arrive at the results for the cavity linewidth and cooperativity C , which are summarized in Tables II and III. From Table III one concludes that for the ideal membrane, i.e. a membrane exhibiting no parasitic scattering, w.r.t. the cooperativity, despite higher g_0 MATE is not advantageous compared to MIM. while MAK is strongly advantageous (at least $2/T_m$ times) compared to other systems.

Another conclusion can be drawn from scrutinizing Fig.5. It is seen that, for the ω_R mode in MIM and MAK, which are the two most advantageous cases, the reflecting membrane is in contact with a field much larger than that at the coupling mirror. This suggests that even very small parasitic scattering may be detrimental for the linewidth and cooperativity for these systems. In the next subsection we will address this matter in detail.

	MATE	MIM	MAK
ω_L	$2/T_m$	1	1/2
ω_R	$T_m/8$	$T_m/4$	1/2

TABLE II. The normalized cavity linewidth κ/κ_0 , $\kappa_0 = cT/l$, for the ω_L and ω_R modes at three configurations: $x \ll x_{\text{int}}$, $|x - l/2| \ll l$, and $l - x \ll x_{\text{int}}$, which are labeled as MATE, MIM, and MAK, respectively. T and T_m are the power transmission coefficients of the coupling mirror and membrane, respectively. The values for MATE and MAK to within a factor of 1/2 hold for the results for the membrane/mirror separation equal to x_{int} . The results are valid for the r-points of the spectrum.

	MATE	MIM	MAK
ω_L	$2/T_m$	1	1/2
ω_R	$2/T_m$	$4/T_m$	$8/T_m^2$

TABLE III. The normalized cooperativity C/C_0 , $C_0 = 16(\omega_c x_{\text{zpf}})^2/(Tcl\gamma_m)$, for the ω_L and ω_R modes at three configurations: $x \ll x_{\text{int}}$, $|x - l/2| \ll l$, and $l - x \ll x_{\text{int}}$, which are labeled as MATE, MIM, and MAK, respectively. T and T_m are the power transmission coefficients of the coupling mirror and membrane, respectively. The values for MATE and MAK to within a factor of 1/2 hold for the results for the membrane/mirror separation equal to x_{int} . The results are valid for the r-points of the spectrum.

B. Linewidth and cooperativity in the presence of parasitic scattering

In order to calculate the linewidth of the system, one can generalize Eq. (8), which is written for the real resonance wave vector, to a resonance equation for the complex wave vector k . Next, one finds the linewidth κ as follows

$$\kappa = -2c\text{Im}[k]. \quad (39)$$

The resonance equation which takes into account the energy decay through the coupling mirror and the parasitic scattering against the membrane reads (see Appendix B)

$$(r_m + e^{-2ik(l-x)-i\varphi_r})(r_m + r^{-1}e^{-2ikx-i\varphi_r}) + 1 - r_m^2 = T_s \quad (40)$$

where $T_s = t_s^2$ is the power scattering coefficient associated with the parasitic scattering (see Eq.(6)) .

Being interested in the r -point of the spectrum in the regime of small damping, we are looking for a solution to (40) written in the form: $k = k_0 + \delta k$ where k_0 is real solution to Eq. (8). Next the problem is linearized with respect to δk . Using this approach and (39) (see Appendix B) for the ω_R mode one finds

$$\kappa_{\text{ext}} = \frac{c}{2} \frac{TT_m/4}{l - x + x_{\text{int}}}, \quad (41)$$

$$\kappa_s = \frac{c}{2} \frac{T_s}{l - x + x_{\text{int}}}, \quad (42)$$

implying for the efficiency:

$$\eta = \frac{TT_m/4}{T_s + TT_m/4}. \quad (43)$$

While, for the ω_L mode:

$$\kappa_{\text{ext}} = \frac{c}{2} \frac{T}{x + x_{\text{int}}}, \quad (44)$$

$$\kappa_s = \frac{c}{2} \frac{T_s}{x + x_{\text{int}}}, \quad (45)$$

implying for the efficiency:

$$\eta = \frac{T}{T_s + T}. \quad (46)$$

Here, $T = t^2$ and $T_m = t_m^2$ are the power transmission coefficients of the coupling mirror and membrane, respectively.

One readily notes that the cooperativity calculated neglecting the parasitic scattering against the membrane should be multiplied by the efficiency to yield the cooperativity calculated taking it into account. Thus using Table III and Eqs. (43) and (46) we arrive at the results listed in Table IV.

The results presented in in Table IV can be summarized as follows. We will discuss the ω_R -regime of MAK, the ω_R -regime of MIM, and the ω_L -regime of MATE. The “standing” of those regimes depends of the position of T_s with respect to $TT_m/4$ and T . At $T_s \ll TT_m/4$, we are back to the dissipation free regime and MAK is advantageous compared to other regimes by a factor of about $1/T_m$. At $TT_m/4 \ll T_s \ll T$, MAK is advantageous compared to MIM by a factor of about $1/T_m$ being advantageous compared to MATE by a factor of about T/T_s . And finally, at $T_s \gg T$, MAK and MATE yields the practically same cooperativity being advantageous compared to MIM by a factor of about $1/T_m$. All in all,

	MATE	MIM	MAK
ω_L	$\frac{2T}{T_m(T_s+T)}$	$\frac{T}{T_s+T}$	$\frac{T/2}{T_s+T}$
ω_R	$\frac{T/2}{T_s+TT_m/4}$	$\frac{T}{T_s+TT_m/4}$	$\frac{2T}{T_m(T_s+TT_m/4)}$

TABLE IV. Cooperativity calculated taking into account the parasitic against the membrane. The normalized cooperativity C/C_0 , $C_0 = 16(\omega_c x_{zpf})^2 / (Tcl\gamma_m)$, for the ω_L and ω_R modes at three configurations: $x \ll x_{\text{int}}$, $|x - l/2| \ll l$, and $l - x \ll x_{\text{int}}$, which are labeled as MATE, MIM, and MAK, respectively. Here $T_s = t_s^2$, $T = t^2$, and $T_m = t_m^2$, are the power scattering coefficient associated with the parasitic scattering and the power transmission coefficients of the coupling mirror and membrane, respectively. The values for MATE and MAK to within a factor of 1/2 hold for the results for the membrane/mirror separation equal to x_{int} . The results are valid for the r-points of the spectrum.

it is seen that, once the parasitic scattering against the membrane is taken into account, in terms of the cooperativity, MAK is the best or at least as good as MATE.

It is instructive to give general expressions for the cooperativity of the ω_R and ω_L modes. Using Eqs. (29), (30), (31), (32), (41), (42), (44), and (45) we find

$$C = \frac{8}{c\gamma_m} \frac{(\omega_c x_{zpf})^2}{x + x_{\text{int}}} \frac{1}{T_s + T} \quad (47)$$

for the ω_L mode and

$$C = \frac{8}{c\gamma_m} \frac{(\omega_c x_{zpf})^2}{l - x + x_{\text{int}}} \frac{1}{T_s + TT_m/4} \quad (48)$$

for the ω_R mode.

C. Efficiency-weighted cooperativity

Multilying Eqs. (47) and (48) with the efficiency given by Eqs. (46) and (43) we find

$$C_\eta = \frac{8}{c\gamma_m} \frac{(\omega_c x_{zpf})^2}{x + x_{\text{int}}} \frac{T}{(T_s + T)^2} \quad (49)$$

for the efficiency-weighted cooperativity of the ω_L mode and

$$C_\eta = \frac{8}{c\gamma_m} \frac{(\omega_c x_{zpf})^2}{l - x + x_{\text{int}}} \frac{TT_m/4}{(T_s + TT_m/4)^2} \quad (50)$$

for the efficiency-weighted cooperativity of the ω_R mode. It is seen that both expressions can be maximized by changing. e.g. T or T_s , to match the internal and external loss.

For the ω_L mode, the maximum is reached at $T = T_s$, which is, in principle, realistic, yielding

$$C_{\eta, \max} = \frac{4}{c\gamma_m} \frac{(\omega_c x_{\text{zpf}})^2}{x + x_{\text{int}}} \frac{1}{T_s}. \quad (51)$$

while, for the ω_R mode, the maximum condition reads

$$TT_m/4 = T_s \quad (52)$$

such that

$$C_{\eta, \max} = \frac{4}{c\gamma_m} \frac{(\omega_c x_{\text{zpf}})^2}{l - x + x_{\text{int}}} \frac{1}{T_s}. \quad (53)$$

Applying the above expression to MIM, we find

$$C_{\eta, \max}^{\text{MIM}} = \frac{8}{c\gamma_m} \frac{(\omega_c x_{\text{zpf}})^2}{l} \frac{1}{T_s} \quad (54)$$

As for MAK and MATE, if we denote the separation between the membrane and the nearest mirror as δ , Eqs. (51) and (53) yields the same result

$$C_{\eta, \max}^{\text{MATE, MAK}} = \frac{4}{c\gamma_m} \frac{(\omega_c x_{\text{zpf}})^2}{\delta + x_{\text{int}}} \frac{1}{T_s}. \quad (55)$$

Comparing Eqs. (54) with (55), since for MAK and MATE, as agreed, $\delta \ll l$, one clearly sees that, w.r.t. the efficiency-weighted cooperativity, MATE and MAK are better than MIM.

VI. MAK AND MATE VS SHORT FABRY-PEROT CAVITY

In the discussion above, we have addressed the problem of the optimal placing of a highly reflecting membrane in a one-sided cavity. We did it for the points of the spectrum, which we called r-points, where g_0 is less affected by the effect of the avoided crossing of the resonance modes of the two subcavities. It was found that MIM is always less effective than MAK and MATE. A remarkable feature of MAK and MATE at the r-points is that the shorter subcavity is on resonance while the longer one is on antiresonance. Actually, MATE can be formally viewed as a short cavity with a synthetic backstop mirror while MAK as that with a synthetic coupling mirror, however with a reservation that, in the regime of interest, the energy of the modes used is not mainly stored in the shorter subcavity. In this context, it is of interest to compare the performance of MAK and MATE, which have membrane/mirror separation δ , with the performance of a δ long one-sided Fabry-Perot (FP) cavity with a membrane used as coupling mirror.

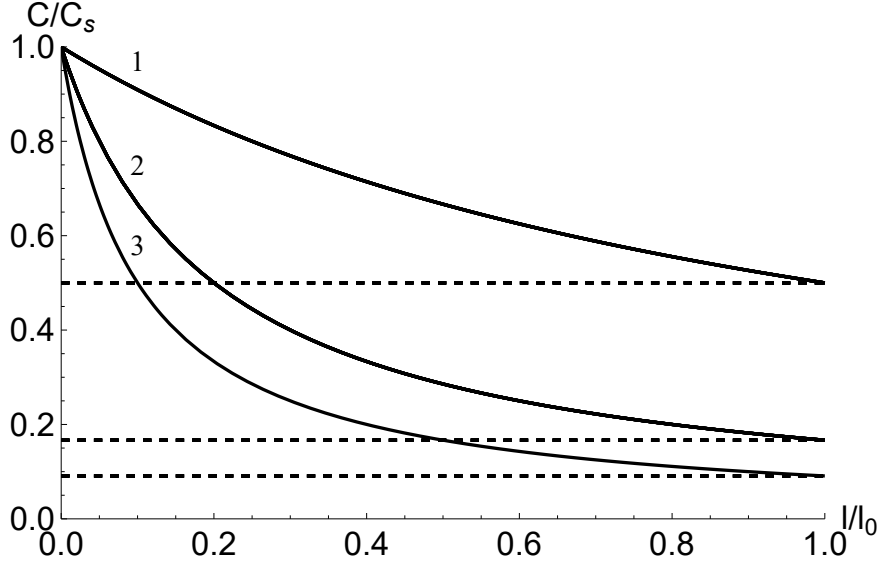


FIG. 6. The normalized cooperativity C_{FP}/C_s of FP (dashed line) and C_{MAK}/C_s of MAK (solid line), plotted as a function of the normalized length of the long cavity l/l_0 , where $l_0 = 4\delta/T_s$ while $C_s = 8(\omega_c x_{\text{zpf}})^2 / (c\gamma_m \delta T_s)$ is the cooperativity of FP in the limit where the loss is fully dominated by the parasitic scattering. Numbers 1, 2, and 3 make the curves plotted for $T_m/T_s = 2, 5,$ and $10,$ respectively. At $l = l_0$, $C_{\text{FP}}/C_s = C_{\text{MAK}}/C_s$. The situation of practical interest where $T_s \gg TT_m/4$ is addressed.

One readily finds the following principle parameters of FP

$$g_0^{\text{FP}} = \frac{\omega_c}{\delta} x_{\text{zpf}} \quad (56)$$

$$\kappa_{\text{ext}}^{\text{FP}} = \frac{cT_m}{2\delta}, \quad \kappa_s^{\text{FP}} = \frac{cT_s}{2\delta}. \quad (57)$$

$$C^{\text{FP}} = \frac{8}{c\gamma_m} \frac{(\omega_c x_{\text{zpf}})^2}{\delta} \frac{1}{T_s + T_m}. \quad (58)$$

$$C_\eta^{\text{FP}} = \frac{8}{c\gamma_m} \frac{(\omega_c x_{\text{zpf}})^2}{\delta} \frac{T_m}{(T_s + T_m)^2} \quad (59)$$

$$C_{\eta, \text{max}}^{\text{FP}} = \frac{4}{c\gamma_m} \frac{(\omega_c x_{\text{zpf}})^2}{\delta} \frac{1}{T_s} \quad (60)$$

Comparing g_0 , i.e (29), (30), and (56), one finds that FP is advantageous by a factor of $\frac{x_{\text{int}} + \delta}{\delta}$. The same factor controls the superiority of FP in the case of the efficiency-weighted cooperativity (c.f. (60) and (55)).

For the cooperativity, we will compare FP with MAK, which, w.r.t. this parameter, is the best of the configurations with the membrane inside the cavity. Thus, we will compare

(58) with (48) rewritten as follows

$$C^{\text{MAK}} = \frac{8}{c\gamma_m} \frac{(\omega_c x_{\text{zpf}})^2}{\delta + lT_m/4} \frac{1}{T_s + TT_m/4}. \quad (61)$$

First, we address the regime of extremely low parasitic scattering where T_s is smaller or about $TT_m/4$, in this regime MAK is strongly advantageous compared to other configurations with a highly reflecting membrane inside the cavity. One readily checks that MAK for not too long cavities, that is

$$l \ll \frac{4\delta}{T_m}, \quad (62)$$

MAK is advantageous over FP by a factor of $\frac{4(T_m+T_s)}{T_m T}$, which can make a few order-of-magnitude gain.

Such a regime, however, is not realistic for currently available systems, where $T_s \gg TT_m/4$. At $T_s \gg TT_m/4$, (58) and (61) can be simplified to find

$$C^{\text{FP}} = \frac{C_s}{1 + \frac{T_m}{T_s}}, \quad (63)$$

$$C^{\text{MAK}} = \frac{C_s}{1 + \frac{l}{\delta} \frac{T_m}{4}} \quad (64)$$

where

$$C_s = \frac{8}{c\gamma_m} \frac{(\omega_c x_{\text{zpf}})^2}{\delta T_s}. \quad (65)$$

is the cooperativity of FP in the limit where the loss is fully dominated by the parasitic scattering. Comparing (63) with (64) shows that, in cavities shorter than $l_0 = 4\delta/T_s$, MAK is better than FP. However that advantage can be appreciable only if $T_s \ll T_m$. Comparison between the systems is also illustrated in Fig. 6. It is worth recalling that throughout this paper we consider MAK at the r-points such that, for MAK, this figure applies only for δ and l corresponding to the r-point condition, i.e. when the shorter subcavity is on resonance while the longer on antiresonance.

VII. OPTIMIZATION OF AN OPTOMECHANICAL SETUP

When discussing above the advantages and disadvantages of various configuration containing a highly reflecting membrane we felt free with manipulating with all parameters of the systems. However, in practice, the experimenter will seek to obtain the highest figure

of merit for their application with a given high-reflecting membrane. Let us the parasitic loss T_s , and the minimum membrane transmission $T_{m,min}$, while allow the membrane transmission be widely tunable above this value via changing the operating wavelength. Beyond the chosen value of the membrane transmission $T_m \geq T_{m,min}$, further quantities are in the hands of the experimenter to choose freely: the separation δ between the membrane the adjacent mirror, the overall length of the cavity l , and the coupling mirror transmission T . The first practical choice the experimenter will have to make is the proximity of the membrane to another mirror. This will determine the separation δ . All schemes favour short δ . A membrane-mirror separation down to $(1.6 \pm 0.8) \mu\text{m}$ was reported in [10]. Once the achievable δ has been chosen, we can discuss optimal choices for the remaining free parameters.

It was shown above that w.r.t. the cooperativity, the best configurations are MAK or FP while w.r.t the weighted cooperativity FP is always the best. For this reason, we will address the optimization of MAK or FP w.r.t. the cooperativity and PF w.r.t the weighted cooperativity.

Starting with the weighted cooperativity of FP, via Eq. (59) and (60), one readily finds that it is maximal when the external loss matches the internal loss, i.e. at $T_m = T_s$. If however, if $T_{m,min} > T_s$, to maximize the weighted cooperativity, one should set $T_m = T_{m,min}$.

When discussing the optimisation w.r.t. the cooperativity we restrict ourselves to the realistic situation where $T_s \gg TT_m/4$ such that Eqs. (63) and (64) and Fig. 6 can be used. First, we see that to maximize the profit from the use of highly reflecting membrane one should use MAK with the cavity shorter than $l_0 = 4\delta/T_s$. Second. as it follows from (64), for the fixed cavity length, a further maximization of the cooperativity is possible by a reduction of the membrane transparency T_m . One can also readily check that the maximal gain of MAK over FP is T_m/T_s . Since T_s can be as small as $10^{-3} - 10^{-4}$ [13–15], such a gain still can be appreciable.

VIII. CONCLUSIONS

We present an analysis of a problem of the optimal position of a highly reflecting membrane in a one-sided cavity. In our analysis, we addressed the coupling constant and the figures of merit of an photomechanical device such as cooperativity and efficiency-weighted

cooperativity. These figures of merit are relevant in different situations, e.g. for optomechanical cooling the cooperativity matters while it is the efficiency-weighted cooperativity that matters for optical sensing of the mechanical subsystem. It was found that the optimal settings for these figures of merit are very different.

In contrast to the previous theoretical considerations of an optical cavity with a membrane inside [1, 2, 10], we have incorporated the parasitic scattering from the membrane in our consideration while neglecting the parasitic scattering from the coupling mirror, which we assume to be much weaker than that from the membrane. We have demonstrated that, in the case of a highly reflecting membrane, even a small amount of parasitic scattering from the membrane may have an essential impact on the cooperativity of the system.

The regimes with the membrane close to the coupling mirror (MATE), close to the backstop mirror (MAK), and close to the cavity center (MIM) were compared. The comparison was done for the points of the spectrum, which we called r-points, where g_0 is less affected by the effect of the avoided crossing of the resonance modes of the two subcavities. A remarkable feature of MAK and MATE at the r-points is that the shorter subcavity is on resonance while the longer one is on antiresonance such that MATE can be viewed as a short cavity with a synthetic backstop mirror while MAK as that with a synthetic coupling mirror. In this context, we compared the optomechanical parameters of MATE and MAK with those of a one-sided Fabry-Perot cavity (FP) with a membrane used as the coupling mirror, its length δ being equal to the separation between the membrane and the adjacent mirror in MAK or MATE.

It has been found that, w.r.t. the coupling constant and the efficiency-weighted cooperativity, FP is the best of all the systems addressed. However, in terms of the cooperativity, the situation is different. Among MIM, MATE and MAK, the latter is always the best though, in some regimes, the performance of MATE can be very close to that of MAK. Comparing MAK with FP, it has been found that each of them can be superior, depending on the parameters of the system. First, in the limit of the very weak parasitic scattering, the regime where $T_s \ll TT_m/4$, MAK is superior over FP by a factor of about $\frac{4(T_m+T_s)}{T_m T}$. Thus, in this regime, MAK would provide an extraordinary performance. However, even a very small amount parasitic scattering from the membrane can essentially suppress the performance of MAK. This happens when T_s is comparable or larger than $TT_m/4$. The situation of practical interest is $T_s \gg TT_m/4$. In this regime, FP can compete with MAK, specifically, for the

cavity length l used in MAK exceeding $l_0 = 4\delta/T_s$, the cooperativity of FP is larger than that of MAK. For shorter cavities, the cooperativity of MAK is larger than that of FP. For the membranes having the parasitic scattering much weaker than the transmission, i.e. for $T_s/T_m \ll 1$ and $l \ll 4\delta/T_s$, this advantage is appreciable being about T_m/T_s .

All in all, in terms of cooperativity, for the opto-mechanical setups using a highly reflecting membrane placed inside an optical cavity, the MAK configuration, is shown here to be advantageous compared to other configurations. However, in this aspect, in a certain regime, the performance of MATE can be very close to that of MAK. In addition, in terms of cooperativity, MAK can also be advantageous compared to FP with the membrane as the coupling mirror with the same membrane/mirror separation as MAK. In the regime of extremely weak parasitic scattering against the membrane, MAK can provide very high cooperativity. Outside of this regime, which currently is a realistic experimental situation, MAK can be tuned to yield a cooperativity larger than that of FP. This advantage can be essential only for a membrane exhibiting the parasitic scattering appreciably weaker than its transmission. If one cares about the efficiency-weighted cooperativity, the use of a highly reflecting membrane is optimal when it serves as the coupling mirror of a FP cavity.

IX. FUNDING

G.E. acknowledges support from the European Union’s Horizon 2020 research and innovation programme under the Marie Skłodowska-Curie grant agreement No. 847523. E.S.P has been supported by VILLUM FONDEN under a Villum Investigator Grant, no. 25880.

X. ACKNOWLEDGMENTS

The authors acknowledge insightful discussions with A. Simonsen and Z. Wang.

XI. DISCLOSURES

The authors declare no conflicts of interest.

XII. DATA AVAILABILITY

Data underlying the results presented in this paper are not publicly available at this time but may be obtained from the authors upon reasonable request.

Appendix A: Reflection from resonance cavity

Consider only the membrane and the backstop mirror in terms of Fig.1, when the $l - x$ long part of the cavity is on resonance, i.e. according to (18)

$$e^{-2ik_0(l-x)-i\varphi_r} = -1. \quad (\text{A1})$$

According to (2), (3) and (4) the complex amplitudes are linked by the following relations

$$B = -Ce^{-2ik(l-x)}, \quad (\text{A2})$$

$$B = t_m e^{i\varphi_t} A + r_m e^{i\varphi_r} C,$$

$$D = r_m e^{i\varphi_r} A + t_m e^{i\varphi_t} C,$$

Eliminating B and C between set (10) and taking into account (A1) we find

$$\frac{D}{A} = -e^{i\varphi_r} \quad (\text{A3})$$

implying that the phase of the signal reflected from a cavity on resonance is independent of the modulus of the reflection coefficient of the coupling mirror.

Appendix B: Coupling constant and decay rate

Equations (1), (2), (3) and (4) lead to the following relations between the complex amplitudes (see Fig. 1)

$$A = -rDe^{2ikx},$$

$$B = -Ce^{-2ik(l-x)}, \quad (\text{B1})$$

$$B = t_m e^{i\varphi_t} A + r_m e^{i\varphi_r} C,$$

$$D = r_m e^{i\varphi_r} A + t_m e^{i\varphi_t} C,$$

which imply the following equation for the resonance wave vector (in general complex)

$$(r_m + e^{-2ik(l-x)-i\varphi_r})(r_m + r^{-1}e^{-2ikx-i\varphi_r}) + t_m^2 = 0. \quad (\text{B2})$$

Since the dissipation is assumed to be weak, to find g_0 we neglect it by setting $r = 1$ and $t_m^2 = 1 - r_m^2$ to find

$$(r_m + e^{-2ik(l-x)-i\varphi_r})(r_m + e^{-2ikx-i\varphi_r}) + 1 - r_m^2 = 0, \quad (\text{B3})$$

which is equivalent to (8). The derivative dk/dx calculated on the resonance using (B3) reads

$$\frac{dk}{dx} = \frac{\omega_c}{c} \frac{e^{-2ik(l-x)-i\varphi_r}(r_m + e^{-2ikx-i\varphi_r}) - e^{-2ikx-i\varphi_r}(r_m + e^{-2ik(l-x)-i\varphi_r})}{(l-x)e^{-2ik(l-x)-i\varphi_r}(r_m + e^{-2ikx-i\varphi_r}) + xe^{-2ikx-i\varphi_r}(r_m + e^{-2ik(l-x)-i\varphi_r})}. \quad (\text{B4})$$

For r-points of ω_R mode where the $l-x$ long subcavity is on resonance while the other subcavity is on antiresonance. i.e. $e^{-2ik_0(l-x)-i\varphi_r} = -1$ and $e^{-2ik_0x-i\varphi_r} = 1$, we find

$$\frac{dk}{dx} = \frac{\omega_c}{c} \frac{r_m}{(l-x)r_m + lt_m^2/4}, \quad (\text{B5})$$

which, in the approximation $t_m^2 \ll 1$, readily yields (30).

For r-points of the ω_L modes where $e^{-2ik_0(l-x)-i\varphi_r} = 1$ and $e^{-2ik_0x-i\varphi_r} = -1$, on the same lines, we obtain (29) as well.

To evaluate the cavity decay rate, we rewrite (B2) as follows

$$(r_m + e^{-2ik(l-x)-i\varphi_r})(r_m + r^{-1}e^{-2ikx-i\varphi_r}) + 1 - r_m^2 = T_s. \quad (\text{B6})$$

We expand (B6) about k_0 , which is the solution to (B3), keeping the lowest term in $t^2 \ll 1$ and $\delta k = k - k_0$, we find

$$\delta k = -\frac{i}{2} \frac{T_s + (1 - r^{-1})e^{-2ik_0x-i\varphi_r}(r_m + e^{-2ik_0(l-x)-i\varphi_r})}{(l-x)e^{-2ik_0(l-x)-i\varphi_r}(r_m + e^{-2ik_0x-i\varphi_r}) + xe^{-2ik_0x-i\varphi_r}(r_m + e^{-2ik_0(l-x)-i\varphi_r})}. \quad (\text{B7})$$

Now, using the above resonance/antiresonance conditions for the subcavities, for ω_R mode, we arrive at the following cavity decay rate:

$$\kappa = -2c\text{Im}[\delta k] = \frac{c}{2} \frac{T_s + (r^{-1} - 1)(1 - r_m)}{(l-x)r_m + lt_m^2/4}, \quad (\text{B8})$$

which, under conditions $1 - r_m \approx T_m/2 \ll 1$ and $1 - r \approx T/2 \ll 1$, readily brings us to (41) and (42).

On the same lines one obtains (44) and (45).

REFERENCES

- [1] A. M. Jayich, J. C. Sankey, B. M. Zwickl, C. Yang, J. D. Thompson, S. M. Girvin, A. A. Clerk, F. Marquardt, and J. G. E. Harris, *New Journal of Physics* **10**, 095008 (2008).
- [2] H. Miao, S. Danilishin, T. Corbitt, and Y. Chen, *Physical Review Letters* **103**, 100402 (2009), publisher: American Physical Society.
- [3] Y. Yanay, J. C. Sankey, and A. A. Clerk, *Physical Review A* **93**, 063809 (2016), publisher: American Physical Society.
- [4] J. D. Thompson, B. M. Zwickl, A. M. Jayich, F. Marquardt, S. M. Girvin, and J. G. E. Harris, *Nature* **452**, 72 (2008).
- [5] D. J. Wilson, C. A. Regal, S. B. Papp, and H. J. Kimble, *Physical Review Letters* **103**, 207204 (2009).
- [6] T. P. Purdy, P.-L. Yu, R. W. Peterson, N. S. Kampel, and C. A. Regal, *Physical Review X* **3**, 031012 (2013).
- [7] D. Mason, J. Chen, M. Rossi, Y. Tsaturyan, and A. Schliesser, *Nature Physics* **15**, 745 (2019).
- [8] N. Kampel, R. Peterson, R. Fischer, P.-L. Yu, K. Cicak, R. Simmonds, K. Lehnert, and C. Regal, *Physical Review X* **7**, 021008 (2017), publisher: American Physical Society.
- [9] A. P. Higginbotham, P. S. Burns, M. D. Urmev, R. W. Peterson, N. S. Kampel, B. M. Brubaker, G. Smith, K. W. Lehnert, and C. A. Regal, *Nature Physics* **14**, 1038 (2018), bandiera_abtest: a Cg_type: Nature Research Journals Number: 10 Primary_atype: Research Publisher: Nature Publishing Group Subject_term: Quantum information;Quantum optics Subject_term_id: quantum-information;quantum-optics.
- [10] V. Dumont, S. Bernard, C. Reinhardt, A. Kato, M. Ruf, and J. C. Sankey, *Optics Express* **27**, 25731 (2019).
- [11] D. J. Wilson, V. Sudhir, N. Piro, R. Schilling, A. Ghadimi, and T. J. Kippenberg, *Nature* **524**, 325 (2015).
- [12] A. K. Tagantsev, I. V. Sokolov, and E. S. Polzik, *Physical Review A* **97**, 063820 (2018).
- [13] X. Chen, C. Chardin, K. Makles, C. Caër, S. Chua, R. Braive, I. Robert-Philip, T. Briant, P.-F. Cohadon, A. Heidmann, T. Jacqmin, and S. Deléglise, *Light: Science & Applications*

6, e16190 (2017).

- [14] G.ENZIAN, Z. WANG, A. SIMONSEN, J. MATHIASSEN, T. VIBEL, Y. TSATURYAN, A. TAGANTSEV, A. SCHLIESSER, and E. S. POLZIK, *Opt. Express* **31**, 13040 (2023).
- [15] F. ZHOU, Y. BAO, J. J. GORMAN, and J. R. LAWALL, *Laser & Photonics Reviews* **2023**, 2300008 (2023), <https://onlinelibrary.wiley.com/doi/pdf/10.1002/lpor.202300008>.